Maastricht University

Optimization of simultaneous multislice EPI for concurrent functional perfusion and BOLD signal measurements at 7T

Citation for published version (APA):

Ivanov, D., Poser, B. A., Huber, L., Pfeuffer, J., & Uludag, K. (2017). Optimization of simultaneous multislice EPI for concurrent functional perfusion and BOLD signal measurements at 7T. *Magnetic Resonance in Medicine*, *78*(1), 121–129. https://doi.org/10.1002/mrm.26351

Document status and date:
Published: 01/07/2017

DOI:
10.1002/mrm.26351

Document Version:
Publisher's PDF, also known as Version of record

Please check the document version of this publication:

• A submitted manuscript is the version of the article upon submission and before peer-review. There can be important differences between the submitted version and the official published version of record. People interested in the research are advised to contact the author for the final version of the publication, or visit the DOI to the publisher's website.
• The final author version and the galley proof are versions of the publication after peer review.
• The final published version features the final layout of the paper including the volume, issue and page numbers.

Link to publication

General rights
Copyright and moral rights for the publications made accessible in the public portal are retained by the authors and/or other copyright owners and it is a condition of accessing publications that users recognise and abide by the legal requirements associated with these rights.

• Users may download and print one copy of any publication from the public portal for the purpose of private study or research.
• You may not further distribute the material or use it for any profit-making activity or commercial gain
• You may freely distribute the URL identifying the publication in the public portal.

If the publication is distributed under the terms of Article 25fa of the Dutch Copyright Act, indicated by the “Taverne” license above, please follow below link for the End User Agreement:

www.umlib.nl/taverne-license

Take down policy
If you believe that this document breaches copyright please contact us at:

repository@maastrichtuniversity.nl

providing details and we will investigate your claim.

Download date: 19 Apr. 2024

FULL PAPER

Magnetic Resonance in Medicine 00:00–00 (2016)

Optimization of Simultaneous Multislice EPI for Concurrent Functional Perfusion and BOLD Signal Measurements at 7T

Dimo Ivanov,[1]* Benedikt A Poser,[1] Laurentius Huber,[2] Josef Pfeuffer,[3] and Kâmil Uludağ[1]

Purpose: To overcome limitations of previous ultra-high-field arterial spin labeling (ASL) techniques concerning temporal resolution and brain coverage by utilizing the simultaneous multi-slice (SMS) approach.

Methods: An optimized, flow-alternating inversion recovery quantitative imaging of perfusion using a single subtraction II scheme was developed that tackles the challenges of 7 tesla (T) ASL. The implementation of tailored labeling radiofrequency pulses reduced the effect of transmit field (B_1^+) inhomogeneities. The proposed approach utilizes an SMS echo-planar imaging (EPI) readout to efficiently achieve large brain coverage.

Results: A pulsed ASL (PASL) technique with large brain coverage is described and optimized that can be applied at temporal resolutions below 2.5 s, similar to those achievable at 1.5 and 3T magnetic field strength. The influences of within- and through-slice acceleration factors and reconstruction parameters on perfusion and blood-oxygenation-level-dependent (BOLD)-signal image and temporal signal-to-noise ratio (SNR) are presented. The proposed approach yielded twice the brain coverage as compared to conventional PASL at 7T, without notable loss in image quality.

Conclusion: The presented SMS EPI PASL at 7T overcomes current limitations in SNR, temporal resolution, and spatial coverage for functional perfusion and BOLD signal as well as baseline perfusion measurements. **Magn Reson Med 000:000–000, 2016.** **© 2016 The Authors Magnetic Resonance in Medicine published by Wiley Periodicals, Inc. on behalf of International Society for Magnetic Resonance in Medicine. This is an open access article under the terms of the Creative Commons Attribution-NonCommercial-NoDerivs License, which permits use and distribution in any medium, provided the original work is properly cited, the use is non-commercial and no modifications or adaptations are made.**

Key words: arterial spin labeling; cerebral blood flow; functional; simultaneous multi-slice; ultra-high field

[1]Department of Cognitive Neuroscience, Faculty of Psychology and Neuroscience, Maastricht University, Maastricht, Netherlands.

[2]SFIM at the National Institute of Mental Health, Bethesda, Maryland, USA.

[3]Siemens Healthcare, MR Application Development, Erlangen, Germany

Grant sponsor: This work was supported by Maastricht University and the Netherlands Organization for Scientific Research (NWO; VIDI grant 452-11-002 to Uludağ).

*Correspondence to: Dimo Ivanov, Department of Cognitive Neuroscience, Faculty of Psychology & Neuroscience, Maastricht University, PO Box 616, 6200MD Maastricht, The Netherlands. E-mail: dimo.ivanov@maastrichtuniversity.nl.

Received 21 December 2015; revised 29 June 2016; accepted 30 June 2016

DOI 10.1002/mrm.26351

Published online 00 Month 2016 in Wiley Online Library (wileyonlinelibrary.com).

© 2016 The Authors Magnetic Resonance in Medicine published by Wiley Periodicals, Inc. on behalf of International Society for Magnetic Resonance in Medicine.

INTRODUCTION

Arterial spin labeling (ASL) is an MRI technique that allows noninvasive quantification of the cerebral blood flow (CBF) by utilizing magnetically labeled arterial blood water as an endogenous tracer (1,2). Measurements of CBF using ASL remain challenging, mainly due to the low microvascular density (~1%–2% of local tissue volume), and hence the low signal-to-noise ratio (SNR) of the perfusion-weighted MRI signal, which necessitates long scan times. An additional challenge for ASL is the limited brain coverage due to T_1 relaxation of labeled blood during the postlabeling delay (PLD) and the image acquisition. Although there have been suggestions for ASL sequences independent of PLD (e.g., (3)), they have not reached maturity to be routinely applied. However, the number of slices for a given readout window can be dramatically increased by employing recent image acquisition techniques, such as simultaneous multi-slice (SMS) or multiband (MB) imaging (4–8).

Recently, SMS has been utilized to increase the brain coverage at little cost in temporal SNR of various MRI techniques, including ASL at 3 tesla (T) (9–12). In the SMS approach, MB composite radiofrequency (RF) pulses are applied to simultaneously excite several spatially distributed imaging slices. The different sensitivity profile of the phased-array coil allows disentangling the signal from the different slices. The key advantage of SMS over conventional parallel imaging methods is that there is no SNR penalty due to k-space undersampling, only SNR reduction due to the *g*-factor imposed by the coil geometry (6). Using CAIPIRINHA (8) - controlled aliasing in parallel imaging results in higher acceleration - the distance between aliasing voxels is increased and higher parallel imaging and/or SMS acceleration factors can be achieved. CAIPIRINHA works by either modulating the phase of the MB excitation pulses (13,14) or adding gradient blips (6). In result, a reduced and more uniform *g*-factor distribution is achieved, thereby increasing the overall SNR. Simultaneous multi-slice imaging (see review in (15)) has demonstrated, for example, improvements for the detection of resting-state networks (7) and dramatically reduced imaging time in diffusion-weighted imaging (16).

Ultra-high field (UHF; 7 Tesla and higher) imaging combined with SMS acquisition offers an attractive approach to increase SNR and coverage of ASL (17): First, image SNR increases with field strength (18,19); second, the longer T_1 relaxation times at higher fields (20,21) amplify the perfusion-related signal changes and allow longer readout acquisition windows; and third, the SMS approach

further increases the spatial coverage. In addition, longer PLD times become feasible, reducing spurious intravascular signal. Further, UHF has proven useful in accurately measuring white-matter perfusion with ASL (22).

Despite these advantages, ASL at UHF has not been widely used in humans due to considerable technical challenges. In particular, B_0 and B_1 inhomogeneities substantially reduce the spatial homogeneity and efficiency of the labeling at UHF (23,24). In addition, the faster T_2^* decay during the echo-planar imaging (EPI) readout results in blurring and resolution loss along the phase-encoding direction (25,26). Parallel imaging shortens the EPI readout and effective echo spacing, yielding a proportional reduction in image blur and geometric distortion due to off-resonance effects (26). The generalized autocalibrating partially parallel acquisitions (GRAPPA) parallel imaging method (27) is often employed due to its use of reference lines data rather than explicitly estimated coil sensitivity profiles. However, subject motion and dynamic B_0 changes, in case the reference lines are collected using segmented EPI over multiple repetition time (TR) periods, can lead to discontinuous SNR and temporal SNR (tSNR) of the accelerated EPI data (28). Polimeni et al. have recently proposed using the fast low-angle excitation echo-planar technique (FLEET) to reorder the reference lines acquisitions such that all segments for a given slice are acquired consecutively as rapidly as possible (28). This was shown to result in substantially higher tSNR and image quality in accelerated EPI. Furthermore, the increased specific absorption rate (SAR) renders widely used techniques at clinical field strengths impractical to be used at UHF, such as background suppression and spin-echo–based approaches (29). In fact, these technical challenges have led to previous implementations of ASL at UHF having only limited brain coverage and/or poor temporal resolution (24,30–35). In particular, the increased SAR at UHF doubles the minimum achievable TR of pseudo-continuous ASL (PCASL) at 3T (36,37), even with low flip-angle readouts (12,33).

In this work, we combine the SMS benefits with perfusion imaging at 7T, in particular for functional experiments. Numerous studies have demonstrated the advantages of UHF for blood-oxygenation-level dependent (BOLD) imaging (38–40), thereby rendering simultaneous CBF and BOLD imaging at 7T especially attractive. To advance (functional) ASL towards its full potential at 7T, we combine an optimized, flow-alternating inversion recovery (FAIR) (41) labeling scheme with an SMS blipped-CAIPI EPI readout. FAIR is SAR-efficient and does not suffer from magnetization transfer effects, which makes it ideally suited for increasing the temporal resolution of ASL at UHF (17,31). In addition, we systematically investigate the influence of within- and through-slice acceleration factors and reconstruction approaches on perfusion and BOLD-signal image and temporal SNR. Because the slice-GRAPPA kernel sizes used in previous SMS ASL studies at 3T and 7T varied, the optimal kernel size for our data was determined. In summary, we developed and optimized ASL techniques for large brain coverage that can be applied at temporal resolutions between 2 and 2.5 s, similar to ASL at 3T. A preliminary account of this work has appeared in abstract form (42,43).

METHODS

Subjects and ASL Acquisition

Experiments were performed on seven healthy volunteers (28 ± 4 years old, 3 female) after obtaining informed consent in accordance with the guidelines of the local ethics committee. Data was acquired on a 7T whole-body MRI scanner with a gradient system achieving a 70 mT/m maximum gradient amplitude, 200 T/m/s maximum slew rate (Siemens Healthcare, Erlangen, Germany), and a 32-channel receive head coil (Nova Medical Inc, Wilmington, MA).

The FAIR labeling scheme was combined in a prototype sequence, with the quantitative imaging of perfusion using a single subtraction II approach (44) and a 2D blipped-CAIPI SMS EPI readout (6). All ASL measurements had 2.5-mm isotropic nominal voxel size, 0.5-mm interslice gap, 80 repetitions, echo time (TE)/TI1/TI2/TR = 11/700/1,800/2,500 ms, echo-spacing 0.53 ms, and either 12 or 24 slices (see next section). The nominal excitation flip angle (67 degrees) was chosen to remain within SAR limits in all measurements. The echo spacing and TE were set as small as possible within the capabilities of the gradient coil. Additional calibration scans were acquired to estimate the blood equilibrium magnetization (M_0) for each of the acquisition variants (described below), with imaging parameters identical to the time-series acquisition but with all ASL preparation pulses set to zero amplitude and TR increased to 20 s (Fig. 1).

With SMS excitation, the N slices in the EPI slice-stack are not acquired one by one in ascending order, but instead the slice-stack is divided into SMS-factor subgroups, each containing N/SMS-factor slices. The n-th slices ($n = 1 \ldots$ N/SMS-factor) in each SMS group are acquired simultaneously—in our case, using ascending slice order (see Figure 1). Either slab-selective or nonselective inversion was performed using an optimized 10-ms time-resampled (tr)-frequency offset corrected inversion (FOCI) pulse (31,45), which achieves high inversion efficiency at 7T despite B_1 inhomogeneities and SAR constraints. In the nonselective case, the spatial extent of the inversion was essentially limited by the transmit field (B_1^+) profile of the head coil. In the selective case, the inversion slab was set to be at least 19.5 mm broader than the imaging volume (at least 9.75 mm on each side). This was done because a mismatch of the inversion slab profiles across the imaging volume would lead to erroneous perfusion values during subtraction. Special care was taken to minimize potential off-resonance effects on the labeling by extending the B_0 shimming volume over the whole brain, including the brainstem.

In order to improve labeling efficiency, the eye centers were taken as reference for the magnet isocenter position (~ level of pons), instead of the eyebrows (~level of basal ganglia) as is typically done. In addition, the necks of the participants were adjusted (in the anterior–posterior direction) to be parallel to the B_0 field by adding cushions below them when necessary. This was done to ensure that the arteries are aligned with the B_0 field as well as possible. Our preliminary test indicated that this procedure not only increased the comfort and reduced motion during the scans but also improved the reliability of the labeling. In order to improve the B_1 efficiency in the major arteries at

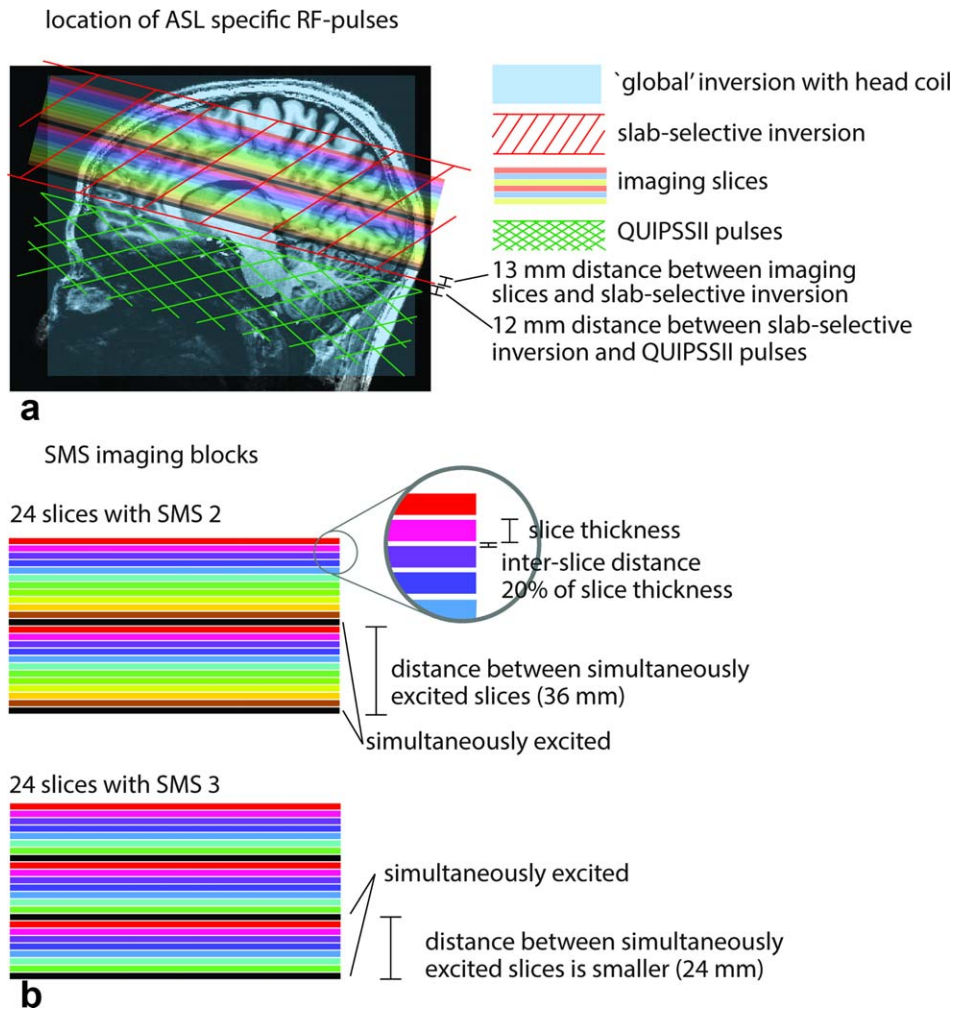

FIG. 1. (A) The SMS ASL acquisition setup overlaid on an anatomical image. The stack of slices with varying colors show the position of the imaging slices. The slices with the same color are acquired simultaneously. Slices with different colors are imaged in an ascending order. The light blue rectangle indicates the extent of a *global* inversion pulse when a head RF coil is used. The red stripe pattern depicts the dimensions of the slab-selective inversion. It was made 13 mm broader (in the superior and inferior direction) than the dimensions of the block of imaging slices. The difference between the global and slab-selective inversion results in the tagged bolus. The green hatch pattern shows the position of the QUIPSSII saturation pulses. (B) A detailed view of the SMS imaging blocks for SMS factors 2 and 3. With increasing SMS factor, the distance between simultaneously excited slices (indicated by the same color) decreases. ASL, arterial spin labeling; RF, radiofrequency; QUIPSSII, quantitative imaging of perfusion using a single subtraction II; SMS, simultaneous multi-slice.

the base of the brain, two rectangular 18*18 cm^2 high-permittivity dielectric pads (2.8:1 weight ratio of calcium titanate in deuterated water) with 5 mm thickness were placed on either side and below the head at the level of the temporal lobes (46). B_1 maps were acquired to guide the choice of transmitter reference voltage, ensuring that the adiabatic condition for the inversion pulse is fulfilled for as large volume across the head as possible.

Sequence and Image Reconstruction Implementation

All ASL acquisitions started with autocalibration: reference scans without magnetization preparation for obtaining the slice-GRAPPA kernel, the GRAPPA reconstruction kernel, or both, depending on whether a through-plane, in-plane acceleration, or both were used. Initial tests indicated that this approach substantially improved the quality of the reconstruction obtained in comparison to when the kernels estimation was done on data with ASL preparation. The SMS scans had 24 slices and 98-mm local inversion slab thickness, whereas the non-SMS acquisitions had 12 slices coinciding with the lower half of the SMS imaging volume and 55-mm slab thickness.

In one volunteer, the optimal in-plane and slice-GRAPPA reconstruction parameters were determined, and the FLEET GRAPPA reference lines acquisition method (28) was compared to the segmented reference lines acquisition approach (see Supporting Figures S1–S5). Based on the findings, the FLEET strategy with a GRAPPA kernel size of [3*2] and a slice-GRAPPA kernel size of {3*3}, whenever applicable, was employed in all experiments reported below.

In six participants, the optimal set of acquisition parameters was investigated by varying the GRAPPA, SMS,

Table 1
Acquisition Parameter Differences Between Datasets Compared (Including Datasets presented in Supporting Figures S1–S5).

GRAPPA Factor	SMS Factor	FOV Shift	Partial Fourier Factor	GRAPPA Reference Lines Acquisition
2	1	No	6/8	FLEET
2	1	No	6/8	Segmented EPI
2	2	3	6/8	FLEET
2	2	3	6/8	Segmented EPI
2	2	2	6/8	FLEET
2	3	3	6/8	FLEET
2	4	2	6/8	FLEET
1	2	2	5/8	No
1	2	3	5/8	No
1	3	2	5/8	No
1	4	3	5/8	No

EPI, echo-planar imaging; FLEET, fast low-angle excitation echo-planar technique; FOV, field of view; GRAPPA, generalized autocalibrating partially parallel acquisitions; SMS, simultaneous multi-slice.

field-of-view (FOV) shift, and partial Fourier factor. For the latter scans, the FLEET reference lines acquisition was applied whenever in-plane acceleration was used. Partial Fourier was used in all cases to shorten the echo time in order to reduce T_2^* weighting, and therefore the susceptibility influence on the perfusion-weighted signal. The in-plane acceleration was limited to 2, and the SMS factor to 4, in order to avoid substantial tSNR loss due to high total acceleration factors. The FOV-shift factors employed for each protocol aimed to optimally utilize the available FOV and thus minimize *g*-factor–related losses in the different SMS protocols. It is worth noting that the SMS imaging volume was fixed; thus, increasing the SMS factor leads to a decrease of the distance between the slices, which have to be unaliased. This distance was 36 mm for SMS 2, 24 mm for SMS 3, and 18 mm for SMS 4. The relevant acquisition parameters of all the acquired datasets are listed in Table 1. Throughout the article, we use the nomenclature GRAPPA factor * SMS factor. The EPI readout lasted with GRAPPA 2 acceleration 15 ms, and without acceleration 25 ms.

Image Analysis

Arterial spin labeling images were corrected for motion and coregistered with SPM 8 (Functional imaging laboratory, University College London, London, UK) without spatial smoothing. Perfusion-weighted images were constructed from the difference between the nonselective and slab-selective images. Surround subtraction results in higher perfusion tSNR but was not applied here to enable better comparison with the values obtained in previous SMS ASL work (9–12). Note, however, that none of the overall results reported below was qualitatively altered when using surround instead of pair-wise subtraction.

Because TI2 slightly differed between the slices of the various ASL acquisitions, the perfusion-weighted maps were corrected using the actual slice-specific TI2 before the CBF calculation. Absolute CBF values were computed for each subject using the approach described in (29). The inversion efficiency was assumed to be 0.95 based on preliminary in vivo measurements for the tr-FOCI RF pulse. The T_1 of blood at 7T was assumed to be 2.1 s based on recent in vivo measurements (47). Only the control images from the ASL time series were used to obtain the BOLD signal data, in order to avoid temporal smoothing when the average of label and control images is employed and facilitate comparison with previous studies. It is important to note that the terms *control (t)SNR* and *BOLD (t)SNR* are identical, but we use the BOLD term to emphasize that a BOLD-weighted time series can be obtained from the ASL data. This becomes especially valid at the high field strength of 7T, where the echo time used in this study (11 ms) approaches the optimal echo time for BOLD imaging (20–25 ms).

The perfusion SNR was estimated by the method described by Feinberg et al. (9): The even- and odd-numbered control image time points from the ASL time series were separately averaged, and the sum and difference of these two images were calculated. The perfusion SNR was calculated as the mean value across a region in the sum image divided by the standard deviation (SD) across the same region in the difference image. Voxel-wise perfusion temporal SNR (tSNR) was calculated as the mean value divided by the SD of the 40-image perfusion-weighted time series. No adjustments to the SNR or tSNR values due to the differences in TI across slices were made. The BOLD tSNR for each scan was obtained by dividing the mean value by the SD of the time series that contained only the control images. The BOLD SNR was computed analogously to the perfusion SNR.

The mean (perfusion or BOLD signal) SNR and tSNR were calculated across the gray matter (GM) of the region common to all ASL acquisitions, that is, the region covered by the motion-corrected non-SMS scan. The GM mask was determined for each subject directly from the intersection of the coregistered and thresholded CBF maps of the individual ASL acquisitions. All voxels with perfusion values between 20 and 120 mL/100 g tissue/min were deemed belonging to GM. The cross-section of all acquisitions was selected instead of only one to avoid a bias toward specific sequence settings and eliminate artifacts in the individual runs. In this way, discrepancies between the EPIs and a GM mask from an anatomical scan due to distortion were avoided. The overall tSNR (or SNR) reduction due to SMS imaging was estimated as 1 minus the ratio of the averaged tSNR (or SNR) for each SMS scan to the non-SMS scan. Statistical analysis was performed on the mean GM CBF values and the perfusion and BOLD (t)SNR using one-way analysis of variance in GraphPad Prism 6 (GraphPad Software, La Jolla, CA) with protocol (2*1, 2*2, 1*2, 1*3, 2*3, 1*4, 2*4) as parameter and Tukey correction for multiple comparisons at 0.05 family-wise significance level.

RESULTS

The dependence of the normalized mean GM perfusion and BOLD (t)SNR over the region covered by all scans on the SMS acceleration factor used is displayed in Figure 2. The results were first averaged across participants and normalized with the mean value from the corresponding parameter of the non-SMS acquisitions (first

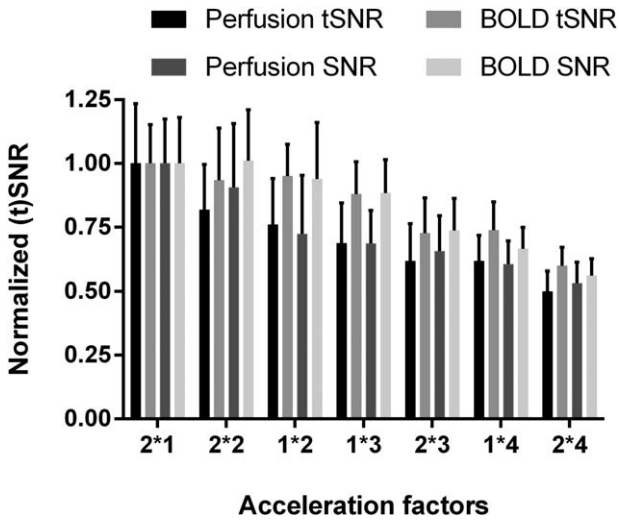

FIG. 2. The dependence of the mean perfusion and blood-oxygenation-level dependent SNR and tSNR on the acquisition parameters used. The mean value over the gray matter covered by all scans was averaged across participants and normalized with respect to the non-SMS scan 2*1. The error bars represent the standard deviation across subjects. The protocols are ordered according to their perfusion tSNR. The acceleration factors nomenclature used is GRAPPA factor * SMS factor.
SMS, simultaneous; tSNR, temporal signal-to-noise ratio multi-slice.

block of bars). Generally, increasing the SMS factor leads to decrease in the (t)SNR for both perfusion- and BOLD-weighted imaging. The (t)SNR dependence on the presence or absence of in-plane acceleration is more variable across SMS factors.

The perfusion tSNR was used as an ordering metric for the acceleration factors. The decrease in perfusion SNR with acceleration factor follows the same trend, albeit with slightly different individual values. In comparison, the BOLD tSNR shows a slightly altered pattern. In particular, the BOLD tSNR of the 1*2 protocol is almost identical to that of the 2*2 one, whereas for perfusion the tSNR of the latter is slightly higher (~7%) than that of the 1*2 case. For the protocols with SMS factors 3 and 4, adding in-plane acceleration leads to additional (t)SNR cost for both BOLD and perfusion. The perfusion tSNR of the 2*1 protocol is statistically significantly higher than the 2*3, 1*3, 1*4, and 2*4 protocols. In contrast, the only other significant difference in perfusion tSNR among all the remaining protocols is between the 2*2 and 2*4 ones, with the latter being smaller. More significant differences exist, when comparing the protocols in terms of BOLD tSNR. The 2*1 protocol has significantly higher BOLD tSNR than the 2*3, 2*4, and 1*4 protocols, whereas the 2*4 protocol has also significantly lower BOLD tSNR than the 2*2, 1*3, and 1*2 ones. The differences in BOLD tSNR between the remaining protocols were not statistically significant. Interestingly, the obtained differences in BOLD SNR between all the protocols were not statistically significant. The perfusion SNR of the 2*1 protocol is significantly higher than that of all other protocols acquired. Further, the 2*2 protocol has significantly higher perfusion SNR than the 1*3, 2*3, 1*4, and 2*4 protocols. The perfusion SNR of the 1*2 protocol is significantly higher than that of the 1*3 and 1*4 protocol, whereas the 1*4 protocol is higher than the 2*4 one. The differences in perfusion SNR between the remaining protocols were not statistically significant.

It is worth pointing out that the (t)SNR losses due to the increase in acceleration factors for the BOLD case are always smaller than the respective losses for perfusion but vary widely in magnitude across protocols. In particular, the normalized perfusion tSNR loss for the 2*2 protocol is $1-0.818=0.182$. The normalized BOLD tSNR loss for the same protocol is 0.066, that is, 36.3% of the loss in perfusion tSNR for this protocol. Using the same approach, the loss in BOLD tSNR is 20.8% of the loss in perfusion tSNR for the 1*2 protocol. Analogously, it is 38.3% for the 1*3 protocol, 71.3% for the 2*3 protocol; 68.4% for the 1*4 protocol; and 80.4% for the 2*4 protocol.

Figure 3 shows CBF maps from one of the subjects acquired with the 2*2 and 1*2 protocols. The lower tSNR of the latter may be due to signal leakage from GM voxels into neighboring non-GM voxels in the phase-encoding direction. Furthermore, the loss of GM delineation in the data obtained without in-plane acceleration, and the corresponding T_2^* blurring, reverse any potential reduction of partial-volume effects offered by the moderate-resolution ASL acquisition. These results underscore the importance of parallel imaging for acquiring high-quality, high-resolution perfusion-weighted images at UHF.

Figure 4 shows the mean GM CBF from the region covered by all scans and averaged across participants. The CBF measured with the non-SMS protocol is higher but not statistically significantly higher than the ones obtained with the other acceleration factors. As mentioned earlier, this can be attributed to the mismatch in

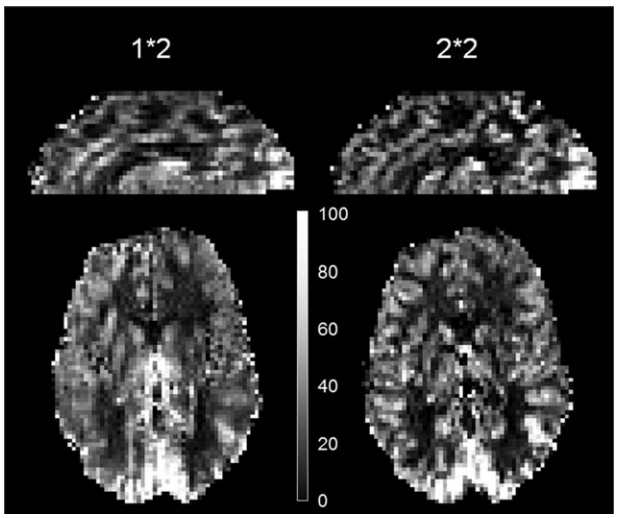

FIG. 3. Single-subject cerebral blood flow maps in mL blood/100 g tissue per min (scaled identically) obtained with the 1*2 protocol on the left and 2*2 protocol on the right. The lack of in-plane acceleration and consequently double effective echo-spacing causes considerable blurring in the phase-encoding direction, reducing not only the image quality but also the temporal signal-to-noise ratio.

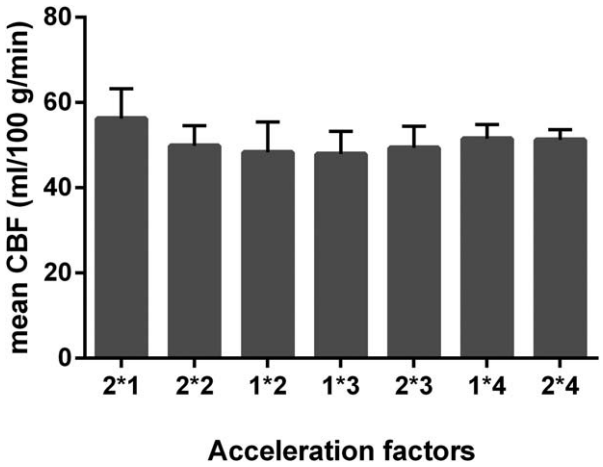

FIG. 4. Dependence of the mean CBF values (in mL blood/100 g tissue per min) on acquisition parameters. The mean value over the gray matter covered by all scans was averaged across participants. The error bars represent the standard deviation across subjects. The acceleration factors nomenclature used is GRAPPA factor * SMS factor.
CBF, cerebral blood flow.

the dimensions of the local inversion slab between the SMS and the conventional acquisitions. The smaller inversion slab of the non-SMS scan permits (venous) blood flowing into the imaging volume from above, thus artificially increasing the perfusion values (48) and the perfusion tSNR. The bright signal in the sagittal sinus in the perfusion-weighted images is another clear indication of the labeling of venous blood. The SMS acquisitions do not yield a statistically significantly different mean CBF compared with each other.

A perfusion tSNR map in three orthogonal views from a representative volunteer is displayed in Figure 5. High tSNR across the GM of the whole volume can be seen. There are no apparent reconstruction artifacts. Due to the optimized FAIR implementation, the proposed PASL approach is not limited by SAR but by sequence timing, which allows it to be used at a temporal resolution previously achievable only at 1.5 and 3T. The coverage is close to whole brain and can be easily extended in the superior direction, if needed, by increasing the number of slices. Nevertheless, the coverage in the inferior direction is more challenging because it can compromise the spatial homogeneity and labeling efficiency of the bolus.

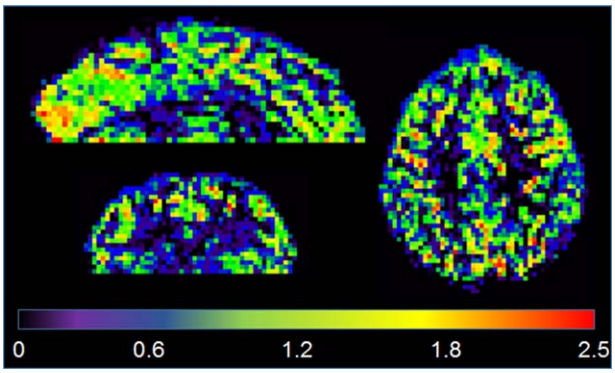

FIG. 5. Perfusion temporal signal-to-noise ratio map of a representative volunteer acquired with the optimal 2*2 protocol. High-fidelity data with close to whole-brain coverage can be acquired at 7 tesla at temporal resolution matching clinical field strengths.

Furthermore, we thoroughly investigated the influence of both acquisition parameters (Supp. Fig. S1) and reconstruction parameters (Supp. Figs. S2-S5) on the perfusion- and BOLD-weighted image SNR and tSNR. Supporting Figures S2 and S3 demonstrate the effects of the GRAPPA reference lines acquisition strategy and of the GRAPPA kernel size on tSNR and SNR, respectively. Supporting Figures S4 and S5 show the respective influence of the slice-GRAPPA kernel size on tSNR and SNR.

DISCUSSION

In this work, an optimized PASL SMS EPI implementation at 7T is presented, which overcomes limitations of previous UHF ASL approaches concerning temporal resolution and brain coverage (24,30–35). The modified tr-FOCI inversion pulse and the use of carefully positioned dielectric pads ensured improved labeling efficiency, whereas the SMS EPI readout offered extended coverage of the brain without increases in TR. In short, SMS offers reduction not only in acquisition time but also in the difference between inversion times across the brain and motion sensitivity (see also (9–12)).

tSNR Dependence on the Acquisition Parameters

Substantial part of the perfusion (t)SNR loss can be attributed to the fact that the perfusion-weighted signal in the SMS scans is less than in the non-SMS one due to differences in the volume of blood labeled. In order to counteract such discrepancies, the 2*2 protocol could serve as a normalization reference for the other SMS protocols. If that is done, the average residual BOLD tSNR losses due to the increase in acceleration factor become 75% of the respective losses for perfusion. This indicates that the acceleration capabilities of perfusion-weighted imaging across a 71.5-mm-thick slab are not as high as for BOLD-weighted imaging. To ensure sufficient perfusion tSNR and simultaneously prevent a rapid drop in BOLD tSNR, the SMS factor should not exceed 3, whereas the total acceleration factor (GRAPPA * SMS) remains below 4. Previous studies using the FAIR approach at 3T have achieved SMS factors up to 5 (9,10), albeit without in-plane acceleration. Simultaneous multi-slice and GRAPPA accelerations have a cumulative (t)SNR cost, with the latter being higher due to the additional (t)SNR penalty from data undersampling (6). Because of the cumulative data undersampling and *g*-factor (t)SNR loss, our total acceleration factor of 4 has to be compared to SMS acceleration of 5 or higher in the aforementioned articles.

A specific reason for the statistically significant tSNR loss (in both perfusion- and BOLD-weighted imaging) with SMS factor above 3 in our data is that the distance between slices that have to be unaliased decreases to only 18 mm. Kim et al., using a 32-channel coil at 3T, demonstrated that whereas 30 mm distance between aliased slices allows good separation, 20 mm distance results in poor performance (10). The similarity in the receive sensitivity profiles of nearby simultaneously excited slices causes a large

g-factor–induced SNR loss when the distance between them becomes too small.

It is important to point out that in the PASL 7T imaging setup, we have a fundamentally different situation than that of 3T SMS ASL papers in which SMS has been previously used to increase the brain coverage without increases in imaging time. The limited brain coverage, as well as the shorter T_2^* at 7T, pose more restrictive limits on the imaging parameters and SMS acceleration factor. Although the perfusion tSNR of the 2*2 protocol is larger than the 1*2 one, due to the reduced blurring of the former, this trend reverses at higher SMS factors: 1*3 and 1*4 have a higher perfusion tSNR than 2*3 and 2*4, respectively. This can be attributed to *g*-factor–related noise enhancement superseding the SNR loss due to blurring at high total acceleration factors. The absolute SNR and tSNR values for perfusion imaging presented here are comparable to the ones achieved with SMS EPI ASL at 3T with an identical number of averages (9,10), albeit with approximately 3.7 and 5.1 times larger voxel volumes than those here. This indicates potentially a higher effective SNR of our implementation for high-resolution perfusion studies. However, several factors may have all contributed to this result, ranging from higher field to shorter TE to receive RF coils arrangement, inversion pulses, and any differences in image reconstruction.

In summary, the protocol with GRAPPA 2 and SMS 2 offers doubling the brain coverage with minimal tSNR penalty for BOLD- and modest tSNR penalty for perfusion-weighted imaging. Moreover, the use of in-plane acceleration in the 2*2 protocol reduces distortions and blurring as compared to the 1*2 case, markedly improving the quality of the perfusion images. Even though higher acceleration factors are possible, the perfusion (t)SNR penalties that are associated with them outweigh the benefits from the reduction of the volume acquisition time, making these suboptimal choices.

PASL versus PCASL at 7T

A direct comparison between our optimized PASL SMS approach and PCASL SMS at 7T was beyond the scope of the study. Nevertheless, we estimate that the SNR efficiency of PASL at 7T with a short TR is comparable to or even higher than that of PCASL at 7T with a long TR, as dictated by SAR limitations for the same brain coverage. The labeling efficiency of PCASL is slightly lower than that of PASL at any field strength, but this effect is expected to be larger at 7T due to the B_1^+ and B_0 inhomogeneities (33). On the other hand, PCASL outperforms PASL in terms of achievable perfusion brain coverage due to the fact that current single-channel transmit head coils at 7T do not allow efficient blood inversion in the lower neck region needed for PASL labeling. This additionally shortens the length of the PASL bolus delivered, lowering the perfusion SNR as elaborated above. For both PCASL and PASL, the application of dielectric pads and the optimized tr-FOCI inversion pulse (for PASL) substantially counteract B_1^+ inhomogeneities but do not necessarily eliminate their effect. A further improvement of the PASL labeling bolus definition and extent as well as PCASL labeling efficiency may be offered by parallel transmission (pTx) techniques (49), such as B_1 shimming using multichannel transmit or dedicated labeling coils (50). In particular, B_1^+ field increase across the whole neck region using a pTx head coil, to fulfill the adiabatic condition for the tr-FOCI inversion pulse, will offer immediate improvements for our approach. In comparison, PCASL labeling improvements will require not only a particular B_1 through the labeling plane but also a specific adjustment of the B_0 field in the same region (24).

Comparison With Other Readout Approaches at 7T

Recently, 2D TurboFLASH (TFL) readouts have been proposed for perfusion imaging at UHF (33) and have even been combined with the SMS approach to increase the brain coverage (12). Due to the low flip angle used, the TFL readout is very SAR-efficient and thus well suited for 7T imaging. However, drawbacks of this approach are its poor temporal resolution (TR twice as long as the one used here) and the fact that it cannot simultaneously acquire CBF and BOLD images, which are the key strengths of our SMS EPI approach.

It is instructive to compare the absolute perfusion SNR and tSNR achieved with the PCASL SMS 2D TFL approach at 7T (12) obtained using very similar hardware. A key difference between the two studies is the echo time achieved: 1.14 ms in (12) versus 11 ms in ours. The short echo time of SMS TFL of around 1 ms minimizes susceptibility contamination of CBF values and makes this approach useful for studies focusing solely on perfusion. Although the spatial perfusion SNR reported by Wang et al. is roughly double of the one achieved with the current method, and similar voxel volume and analysis procedures were used, the perfusion tSNR is essentially the same as the one achieved here. The relatively low tSNR of the 2D TFL approach may be related to increased physiological variations during the 330-ms readout. However, SMS TFL may be better than our approach for high-resolution and white matter perfusion imaging. The very short TE achievable, irrespective of the image matrix size, diminishes the perfusion signal loss in white matter present in other ASL approaches due to the short T_2^* of the latter at 7T. For single-shot EPI readouts, the echo time for high-resolution imaging increases rapidly with the image matrix size but not for TFL.

Studies suggest that three-dimensional (3D) MRI sequences, such as the 3D gradient and spin echo (3D GRASE) technique, provide better SNR when compared to single-TI 2D ASL for whole-brain acquisition (51,52). However, the long time required for data collection in 3D GRASE causes severe through-plane (in the second phase-encoding direction) blurring due to T_2 decay. In effect, the slice resolution is typically kept low to reduce the artifactual contributions of perfusion values from other slices due to blurring. Shortening the acquisition window (i.e., the echo-train length) can be accomplished by parallel imaging and/or multishot acquisition and minimizes through-plane blurring. However, this comes at the cost of either (t)SNR losses or increases in scan time with decreases in temporal resolution. At 7T, T_2 of blood gets shorter than at lower field strengths; therefore, the readout train needs to become even shorter to avoid increased blurring. Finally, the increased SAR and B_1 inhomogeneity at 7T further limit the utility of 3D GRASE for ASL at UHF.

Another 3D ASL approach suitable for 7T is 3D EPI (34). Because it uses low flip-angle RF pulses for the EPI readouts, it has low SAR and is less affected by B_1^+ inhomogeneities. Indeed, a direct comparison between the 2D SMS-EPI and 3D EPI for ASL at 7T will be very instructive but is beyond the scope of this work.

Significance of the Findings for Other fMRI Techniques

The current findings for optimal acquisition and reconstruction parameters in SMS FAIR ASL at 7T may extend to other (multi-TI) PASL approaches such as Look-Locker ASL, as well as to other inversion recovery EPI techniques (e.g., vascular space occupancy (VASO) (53) and slab-selective slab-inversion VASO (54)), using the same field and RF coil. The consistently higher temporal stability of FLEET over the segmented reference lines acquisition will benefit all ASL techniques using GRAPPA and 2D EPI readouts at any field strength (see Supporting Figures S1–S3). Despite the suboptimal echo time for BOLD imaging used here, it is possible that the optimal GRAPPA and slice-GRAPPA kernels reported may also translate to standard BOLD functional MRI (fMRI) at 7T, with similar spatial and temporal resolution if the same reconstruction algorithms are used (see Supporting Figures S2–S5). The BOLD tSNR dependence on the slice-GRAPPA kernel size did not always follow the perfusion tSNR behavior. This indicates that the optimal slice-GRAPPA reconstruction kernel for BOLD fMRI may depend on the specific SMS acceleration factor and distance between the slices that need to be unaliased.

CONCLUSION

The proposed SMS ASL approach increases the brain coverage at 7T at a small tSNR cost for SMS factor of 2 compared to a conventional 2D PASL acquisition. A combination of FLEET GRAPPA-2 and SMS-2 acceleration constitutes an optimal parameter set, taking into account brain coverage, tSNR, and artefact levels for moderate-resolution PASL acquisitions at 7T. The technique proves useful for both functional and baseline perfusion measurements, bringing ASL at UHF closer to its full potential. The optimal reconstruction parameters determined in this study may also find application in other fMRI techniques at 7T, such as VASO and BOLD imaging.

ACKNOWLEDGMENT

We thank Dr. Stephen Cauley (Massachusetts General Hospital) for sharing the interface of their online image reconstruction (part of the package that can be requested at: https://www.nmr.mgh.harvard.edu/software/c2p/sms) for use in our SMS ASL sequence. The authors are indebted to Professor Dr. Andrew Webb for providing the dielectric pads used in this study.

REFERENCES

1. Detre JA, Leigh JS, Williams DS, Koretsky AP. Perfusion imaging. Magn Reson Med 1992;23:37–45.
2. Williams DS, Detre JA, Leigh JS, Koretsky AP. Magnetic resonance imaging of perfusion using spin inversion of arterial water. Proc Natl Acad Sci U S A 1992;89:212–216.
3. Wong EC, Cronin M, Wu WC, Inglis B, Frank LR, Liu TT. Velocity-selective arterial spin labeling. Magn Reson Med 2006;55:1334–1341.
4. Larkman DJ, Hajnal JV, Herlihy AH, Coutts GA, Young IR, Ehnholm G. Use of multicoil arrays for separation of signal from multiple slices simultaneously excited. J Magn Reson Imaging 2001;13:313–317.
5. Moeller S, Yacoub E, Olman CA, Auerbach E, Strupp J, Harel N, Ugurbil K. Multiband multislice GE-EPI at 7 tesla, with 16-fold acceleration using partial parallel imaging with application to high spatial and temporal whole-brain fMRI. Magn Reson Med 2010;63:1144–1153.
6. Setsompop K, Gagoski BA, Polimeni JR, Witzel T, Wedeen VJ, Wald LL. Blipped-controlled aliasing in parallel imaging for simultaneous multislice echo planar imaging with reduced g-factor penalty. Magn Reson Med 2012;67:1210–1224.
7. Feinberg DA, Moeller S, Smith SM, Auerbach E, Ramanna S, Gunther M, Glasser MF, Miller KL, Ugurbil K, Yacoub E. Multiplexed echo planar imaging for sub-second whole brain FMRI and fast diffusion imaging. PloS One 2010;5:e15710.
8. Breuer FA, Blaimer M, Heidemann RM, Mueller MF, Griswold MA, Jakob PM. Controlled aliasing in parallel imaging results in higher acceleration (CAIPIRINHA) for multi-slice imaging. Magn Reson Med 2005;53:684–691.
9. Feinberg DA, Beckett A, Chen L. Arterial spin labeling with simultaneous multi-slice echo planar imaging. Magn Reson Med 2013;70: 1500–1506.
10. Kim T, Shin W, Zhao T, Beall EB, Lowe MJ, Bae KT. Whole brain perfusion measurements using arterial spin labeling with multiband acquisition. Magn Reson Med 2013;70:1653–1661.
11. Li X, Wang D, Auerbach EJ, Moeller S, Ugurbil K, Metzger GJ. Theoretical and experimental evaluation of multi-band EPI for high-resolution whole brain pCASL Imaging. Neuroimage 2015;106:170–181.
12. Wang Y, Moeller S, Li X, Vu AT, Krasileva K, Ugurbil K, Yacoub E, Wang DJ. Simultaneous multi-slice Turbo-FLASH imaging with CAIPIRINHA for whole brain distortion-free pseudo-continuous arterial spin labeling at 3 and 7T. Neuroimage 2015;113:279–288.
13. Glover GH. Phase-offset multiplanar (POMP) volume imaging: a new technique. J Magn Reson Imaging 1991;1:457–461.
14. Souza SP, Szumowski J, Dumoulin CL, Plewes DP, Glover G. SIMA: simultaneous multislice acquisition of MR images by Hadamard-encoded excitation. J Comput Assist Tomogr 1988;12:1026–1030.
15. Barth M, Breuer F, Koopmans PJ, Norris DG, Poser BA. Simultaneous multislice (SMS) imaging techniques. Magn Reson Med 2016;75: 63–81.
16. Setsompop K, Cohen-Adad J, Gagoski BA, Raij T, Yendiki A, Keil B, Wedeen VJ, Wald LL. Improving diffusion MRI using simultaneous multi-slice echo planar imaging. Neuroimage 2012;63:569–580.
17. Gardener AG, Gowland PA, Francis ST. Implementation of quantitative perfusion imaging using pulsed arterial spin labeling at ultra-high field. Magn Reson Med 2009;61:874–882.
18. Pohmann R, Speck O, Scheffler K. Signal-to-noise ratio and MR tissue parameters in human brain imaging at 3, 7, and 9.4 tesla using current receive coil arrays. Magn Reson Med 2016;75:801–809.
19. Norris DG. High field human imaging. J Magn Reson Imaging 2003; 18:519–529.
20. Wright PJ, Mougin OE, Totman JJ, Peters AM, Brookes MJ, Coxon R, Morris PE, Clemence M, Francis ST, Bowtell RW, Gowland PA. Water proton T1 measurements in brain tissue at 7, 3, and 1.5 T using IR-EPI, IR-TSE, and MPRAGE: results and optimization. MAGMA 2008;21:121–130.
21. Rooney WD, Johnson G, Li X, Cohen ER, Kim SG, Ugurbil K, Springer CS Jr. Magnetic field and tissue dependencies of human brain longitudinal 1H2O relaxation in vivo. Magn Reson Med 2007; 57:308–318.
22. Gardener AG, Jezzard P. Investigating white matter perfusion using optimal sampling strategy arterial spin labeling at 7 Tesla. Magn Reson Med 2015;73:2243–2248.
23. Teeuwisse WM, Webb AG, van Osch MJR. Arterial spin labeling at ultra-high field: all that glitters is not gold. Int J Imag Syst Tech 2010;20:62–70.
24. Luh WM, Talagala SL, Li TQ, Bandettini PA. Pseudo-continuous arterial spin labeling at 7 T for human brain: estimation and correction for off-resonance effects using a prescan. Magn Reson Med 2013;69: 402–410.
25. Farzaneh F, Riederer SJ, Pelc NJ. Analysis of T2 limitations and off-resonance effects on spatial resolution and artifacts in echo-planar imaging. Magn Reson Med 1990;14:123–139.

26. de Zwart JA, van Gelderen P, Golay X, Ikonomidou VN, Duyn JH. Accelerated parallel imaging for functional imaging of the human brain. NMR Biomed 2006;19:342–351.
27. Griswold MA, Jakob PM, Heidemann RM, Nittka M, Jellus V, Wang J, Kiefer B, Haase A. Generalized autocalibrating partially parallel acquisitions (GRAPPA). Magn Reson Med 2002;47:1202–1210.
28. Polimeni JR, Bhat H, Witzel T, Benner T, Feiweier T, Inati SJ, Renvall V, Heberlein K, Wald LL. Reducing sensitivity losses due to respiration and motion in accelerated echo planar imaging by reordering the autocalibration data acquisition. Magn Reson Med 2016; 75:665–679.
29. Alsop DC, Detre JA, Golay X, et al. Recommended implementation of arterial spin-labeled perfusion MRI for clinical applications: a consensus of the ISMRM perfusion study group and the European consortium for ASL in dementia. Magn Reson Med 2015;73:102–116.
30. Ghariq E, Teeuwisse WM, Webb AG, van Osch MJ. Feasibility of pseudocontinuous arterial spin labeling at 7 T with whole-brain coverage. MAGMA 2012;25:83–93.
31. Bause J, Ehses P, Mirkes C, Shajan G, Scheffler K, Pohmann R. Quantitative and functional pulsed arterial spin labeling in the human brain at 9.4 t. Magn Reson Med 2016;75:1054–1063.
32. Pfeuffer J, Adriany G, Shmuel A, Yacoub E, Van De Moortele PF, Hu X, Ugurbil K. Perfusion-based high-resolution functional imaging in the human brain at 7 tesla. Magn Reson Med 2002;47:903–911.
33. Zuo Z, Wang R, Zhuo Y, Xue R, St Lawrence KS, Wang DJ. Turbo-FLASH based arterial spin labeled perfusion MRI at 7 T. PloS One 2013;8:e66612.
34. Hall EL, Gowland P, Francis ST. 3D-EPI ASL at ultra high field. In Proceedings of the 18th Annual Joint Annual Meeting ISMRM-ESMRMB in Stockholm, Sweden, 2010. p. 517.
35. Zimmer F, O'Brien K, Bollmann S, Pfeuffer J, Heberlein K, Barth M. Pulsed arterial spin labeling at ultra-high field with a B 1 (+) -optimised adiabatic labeling pulse. MAGMA 2016;29:463–473.
36. Wu WC, Fernandez-Seara M, Detre JA, Wehrli FW, Wang J. A theoretical and experimental investigation of the tagging efficiency of pseudocontinuous arterial spin labeling. Magn Reson Med 2007;58:1020–1027.
37. Dai W, Garcia D, de Bazelaire C, Alsop DC. Continuous flow-driven inversion for arterial spin labeling using pulsed radio frequency and gradient fields. Magn Reson Med 2008;60:1488–1497.
38. Uludag K, Muller-Bierl B, Ugurbil K. An integrative model for neuronal activity-induced signal changes for gradient and spin echo functional imaging. Neuroimage 2009;48:150–165.
39. Donahue MJ, Hoogduin H, van Zijl PC, Jezzard P, Luijten PR, Hendrikse J. Blood oxygenation level-dependent (BOLD) total and extravascular signal changes and DeltaR2* in human visual cortex at 1.5, 3.0 and 7.0 T. NMR Biomed 2011;24:25–34.
40. van der Zwaag W, Francis S, Head K, Peters A, Gowland P, Morris P, Bowtell R. fMRI at 1.5, 3 and 7 T: characterising BOLD signal changes. Neuroimage 2009;47:1425–1434.
41. Kim SG. Quantification of relative cerebral blood flow change by flow-sensitive alternating inversion recovery (FAIR) technique: application to functional mapping. Magn Reson Med 1995;34: 293–301.
42. Ivanov D, Poser BA, Huber L, Pfeuffer J, Uludag K. Whole-brain perfusion measurements at 7T using pulsed arterial spin labeling and simultaneous multi-slice multi-echo echo planar imaging. In Proceedings of the 22nd Annual Meeting of ISMRM Meeting & Exhibition in Milan, Italy, 2014. p. 2698.
43. Ivanov D, Huber L, Pfeuffer J, Uludag K, Poser BA. Evaluation of parallel imaging acquisition and reconstruction parameters on the tSNR of arterial spin labeling SMS-EPI at 7T. ISMRM Workshop on Simultaneous Multi-Slice Imaging: Neuroscience & Clinical Applications. Pacific Grove, California, USA, 2015.
44. Wong EC, Buxton RB, Frank LR. Quantitative imaging of perfusion using a single subtraction (QUIPSS and QUIPSS II). Magn Reson Med 1998;39:702–708.
45. Hurley AC, Al-Radaideh A, Bai L, Aickelin U, Coxon R, Glover P, Gowland PA. Tailored RF pulse for magnetization inversion at ultra-high field. Magn Reson Med 2010;63:51–58.
46. Teeuwisse WM, Brink WM, Webb AG. Quantitative assessment of the effects of high-permittivity pads in 7 Tesla MRI of the brain. Magn Reson Med 2012;67:1285–1293.
47. Zhang X, Petersen ET, Ghariq E, De Vis JB, Webb AG, Teeuwisse WM, Hendrikse J, van Osch MJ. In vivo blood T(1) measurements at 1.5 T, 3 T, and 7 T. Magn Reson Med 2013;70:1082–1086.
48. Cavusoglu M, Pfeuffer J, Ugurbil K, Uludag K. Comparison of pulsed arterial spin labeling encoding schemes and absolute perfusion quantification. Magn Reson Imaging 2009;27:1039–1045.
49. Setsompop K, Alagappan V, Gagoski B, et al. Slice-selective RF pulses for in vivo B1 + inhomogeneity mitigation at 7 tesla using parallel RF excitation with a 16-element coil. Magn Reson Med 2008;60: 1422–1432.
50. Talagala SL, Ye FQ, Ledden PJ, Chesnick S. Whole-brain 3D perfusion MRI at 3.0 T using CASL with a separate labeling coil. Magn Reson Med 2004;52:131–140.
51. Gunther M, Oshio K, Feinberg DA. Single-shot 3D imaging techniques improve arterial spin labeling perfusion measurements. Magn Reson Med 2005;54:491–498.
52. Fernandez-Seara MA, Edlow BL, Hoang A, Wang J, Feinberg DA, Detre JA. Minimizing acquisition time of arterial spin labeling at 3T. Magn Reson Med 2008;59:1467–1471.
53. Lu H, Golay X, Pekar JJ, van Zijl PCM. Functional magnetic resonance Imaging based on changes in vascular space occupancy. Magn Reson Med 2003;50:263–274.
54. Huber L, Ivanov D, Krieger SN, Streicher MN, Mildner T, Poser BA, Moller HE, Turner R. Slab-selective, BOLD-corrected VASO at 7 Tesla provides measures of cerebral blood volume reactivity with high signal-to-noise ratio. Magn Reson Med 2014;72:137–148.

SUPPORTING INFORMATION

Additional supporting information may be found in the online version of this article.

SUP. FIG. S1. The influence of the GRAPPA reference line acquisition strategy on the perfusion (left panel) and BOLD tSNR (right panel) for the non-SMS scan (2 * 1). The images within a panel are identically windowed with the scale located below. The images on the left-hand side are acquired with the Segmented strategy, whereas the ones on the right-hand side are acquired using the FLEET approach.

SUP. FIG. S2. The influence of the GRAPPA reference line acquisition strategy (FLEET - solid colors, and Segmented - hatch patterns) on the perfusion tSNR in black (left y-axis) and BOLD tSNR in grey (right y-axis) for several combinations of acquisition and reconstruction parameters. The protocol parameters are listed below the x-axis according to the following nomenclature: GRAPPA factor * SMS factor; [GRAPPA kernel size in read direction * GRAPPA kernel size in phase-encoding (PE) direction]; {Slice-GRAPPA kernel size}.

SUP. FIG. S3. The influence of the GRAPPA reference line acquisition strategy (FLEET - solid colors, and Segmented - hatch patterns) on the perfusion SNR in black (left y-axis) and BOLD SNR in grey (right y-axis) for several combinations of acquisition and reconstruction parameters. The protocol parameters are listed below the x-axis according to the following nomenclature: GRAPPA factor * SMS factor; [GRAPPA kernel size in read direction * GRAPPA kernel size in phase-encoding (PE) direction]; {Slice-GRAPPA kernel size}.

SUP. FIG. S4. The influence of the slice-GRAPPA kernel size (3*3 - solid colors, 5*5 - fine hatch patterns, 7*7 - coarse hatch patterns) on the perfusion tSNR in black (left y-axis) and BOLD tSNR in grey (right y-axis) for several combinations of acquisition and reconstruction parameters. The FLEET reference lines acquisition strategy was employed in all cases. The protocol parameters are listed below the x-axis according to the following nomenclature: GRAPPA factor * SMS factor; [GRAPPA kernel size in read-out direction * GRAPPA kernel size in phase-encoding direction].

SUP. FIG. S5. The influence of the slice-GRAPPA kernel size (3*3 - solid colors, 5*5 - fine hatch patterns, 7*7 - coarse hatch patterns) on the perfusion SNR in black (left y-axis) and BOLD SNR in grey (right y-axis) for several combinations of acquisition and reconstruction parameters. The FLEET reference lines acquisition strategy was employed in all cases. The protocol parameters are listed below the x-axis according to the following nomenclature: GRAPPA factor * SMS factor; [GRAPPA kernel size in read-out direction * GRAPPA kernel size in phase-encoding direction].